# Numerical investigations of the impact of buffer germanium composition and low cost fabrication of Cu2O on AZO/ZnGeO/Cu2O solar cell performances

Christyves Chevallier, Sourav Bose, Sidi Ould Saad Hamady, Nicolas Fressengeas

EPJ Photovoltaics **12**, 3 (2021)

https://doi.org/10.1051/epjpv/2021003

Available online at:
www.epj-pv.org

REGULAR ARTICLE

OPEN ACCESS

# Numerical investigations of the impact of buffer germanium composition and low cost fabrication of $Cu_2O$ on AZO/ZnGeO/$Cu_2O$ solar cell performances

Christyves Chevallier*, Sourav Bose, Sidi Ould Saad Hamady, and Nicolas Fressengeas

Université de Lorraine, CentraleSupélec, LMOPS, F-57000 Metz, France

Received: 11 January 2021 / Received in final form: 23 April 2021 / Accepted: 21 May 2021

**Abstract.** Numerical simulations of AZO/$Zn_{1-x}Ge_xO$/$Cu_2O$ solar cell are performed in order to model for the first time the impact of the germanium composition of the ZnGeO buffer layer on the photovoltaic conversion efficiency. The physical parameters of the model are chosen with special care to match literature experimental measurements or are interpolated using the values from binary metal oxides in the case of the new $Zn_{1-x}Ge_xO$ compound. The solar cell model accuracy is then confirmed thanks to the comparison of its predictions with measurements from the literature that were done on experimental devices obtained by thermal oxidation. This validation of the AZO/$Zn_{1-x}Ge_xO$/$Cu_2O$ model then allows to study the impact of the use of the low cost, environmental friendly and industrially compatible spray pyrolysis process on the solar cell efficiency. To that aim, the $Cu_2O$ absorber layer parameters are adjusted to typical values obtained by the spray pyrolysis process by selecting state of the art experimental data. The analysis of the impact of the absorber layer thickness, the carrier mobility, the defect and doping concentration on the solar cell performances allows to draw guidelines for ZnGeO/$Cu_2O$ thin film photovoltaic device realization through spray pyrolysis.

**Keywords:** Photovoltaic / solar cell model / numerical simulation / metal oxide / $Cu_2O$ / ZnGeO / germanium composition / low cost fabrication

Among the potential future photovoltaic technologies, metal oxide materials are promising to develop thin film solar cells based on low toxicity and earth abundant elements in order to further reduce the production cost and environmental impact. Besides the use of metal oxides in transparent conductive electrodes, photovoltaic technologies can benefit from the advantages of these materials to produce all oxide solar cell structures [1]. Several candidate materials are currently being explored to develop metal oxide absorber: materials such as $BiFeO_3$, $Fe_2O_3$ or $Co_3O_4$ [2]. Among them, copper oxide ($Cu_2O$) has been the most popular one during the past decades [3] because it exhibits properties that are interesting for photovoltaic applications. Indeed, copper oxide is a *p*-type semi-conductor and benefits from a large absorption coefficient ($\alpha > 10^5\ cm^{-1}$) [4] and high electrical properties (Hall mobility higher than $100\ cm^2\ V^{-1}\ s^{-1}$ and carrier concentration ranging from $10^{13}$ to $10^{16} cm^{-3}$ [5]). Even though the large bandgap value of 2.1 eV of $Cu_2O$ limits its theoretical photovoltaic conversion efficiency around 20% (Shockley-Queisser limit) [6], copper oxide combines both interesting electrical and optical properties for a low toxicity, low cost and earth abundant [7] photovoltaic application.

During the past decade, important work on the optimisation of $Cu_2O$ based photovoltaics was performed [3]. The last improvements concern the optimization of the band alignment of the structure by carefully selecting the buffer layer material. In fact, one limitation of the use of $Cu_2O$ as the absorber layer is its low electron affinity $\chi = 2.1$ eV which creates a conduction band offset with the buffer layer which is typically made of zinc oxide ($\chi = 4.4$ eV) [8] or titanium oxide ($\chi = 4.1$ eV) [9]. Previous simulations show that the reduction of the electron affinity of the buffer layer to 3.2 eV enhances the efficiency of the device [10]. Thus, in order to decrease the conduction band offset of $Cu_2O$ solar cells, a zinc germanium oxide compound was experimentally introduced as the buffer layer to benefit from the low electron affinity of germanium oxide which results in an optimum 8.1% efficiency device [11].

It is worth mentioning that the most efficient $Cu_2O$ photovoltaic devices were obtained thanks to a thermal oxidation process from copper foils, a well established

* e-mail: christyves.chevallier@univ-lorraine.fr

method to grow high quality copper oxide. Despite the excellent material properties of the resulting $Cu_2O$, the high energy consumption of the thermal oxidation done under high temperatures (>1000 °C) for several hours limits its application for a low cost industrial scale elaboration of solar devices. In order to reach the photovoltaic market, several manufacturing processes using large area capable, low cost and environmental friendly methods are currently explored such as sputtering [12–14] or electrodeposition [15,16]. Among the low cost technologies, the spray pyrolysis process is of high interest and currently the subject of increasing research for the production of $Cu_2O$ solar cells [17–19]. Promising results have already been shown with $TiO_2/Cu_2O$ or $ZnO/Cu_2O$ heterojunctions. However, the efficiency of the devices grown by spray pyrolysis is still limited below 1%. In order to improve the performances of metal oxide solar cells obtained by spray pyrolysis, further optimisation of the elaboration process has to be done by decreasing impurities levels in the material [20] or prevent unwanted copper oxide phases at the junction interface. The latter issue is well known for $Cu_2O$ heterojunctions [21]. Besides the optimization of the elaboration process, an important work on the design of the structure remains to be done by taking into account the specificity of the spray pyrolysis process.

The work outlined in this paper is thus focused on numerical simulations of $AZO/ZnGeO/Cu_2O$ heterojunctions. In a first part, a numerical model of the $AZO/ZnGeO/Cu_2O$ solar cell is defined using physical parameters carefully chosen from experimental measurements from the literature. Simulation results are then compared with the performances of the record experimental solar cells [11] which is referred as the reference device in the present paper, and allows for the first time the study of the impact of the germanium composition of the ZnGeO buffer layer. In a second part, the effect of the absorber layer parameters are investigated by taking into account the constraints of the spray pyrolysis process on the $Cu_2O$ material quality. From this study, a set of guidelines for the development of efficient metal oxide photovoltaic devices by spray pyrolysis are drawn.

## 1 The ZnGeO/$Cu_2O$ solar cell model

The solar cell model described in this section is developed to reproduce the experimental results obtained with a structure based on a 200 nm thick aluminum zinc oxide (AZO) and a 60 nm $Zn_{1-x}Ge_xO$ buffer deposited by Pulsed Laser Deposition (PLD) on top of a 200 µm $Cu_2O$ absorber layer obtained by thermal oxidation [11]. The modeling is performed through numerical simulation by solving the Poisson and continuity equations (using Silvaco ATLAS software version 5.19.20.R) in order to extract the solar cell characteristics, namely its short circuit current $J_{SC}$, its open circuit voltage $V_{OC}$, its fill factor $FF$ and its efficiency $\eta$.

Previous numerical models of copper based photovoltaic devices have shown the importance to introduce interface defects at the junction to account for the presence of unwanted copper oxide phases and reproduce the experimental characteristics of the solar cell [10]. The solar cell presented in this paper uses a similar model by introducing an interface layer and a defect layer at the junction. Electrical defects are taken into account through a Shockley-Read-Hall (SRH) recombination model with a Gaussian distribution of recombination centers at midgap energies and a width of 0.1 eV in each layer of the structure. The only exception being the interface layer at the junction for which two discrete trap levels are defined at $0.25 \times E_g^{IL}$ and $0.75 \times E_g^{IL}$ energies with respect to the valence band, $E_g^{IL}$ being the bandgap energy of the interface layer. For an accurate modeling of the structure, the physical properties of the materials are chosen as rigorously as possible from experimental measurements through a precise selection from a literature review described in the following sections. A summary of the model parameters used is shown in Table 1 and their choice is discussed in the following.

### 1.1 Physical parameters of the $Cu_2O$ absorber layer

The description of the solar cell structure starts with the definition of the physical parameters of the absorber layer from a comprehensive literature survey. Data is selected from the measurements done on $Cu_2O$ films obtained by the same thermal oxidation process as was used for the photovoltaic device from the work of Minami et al. [11] that we have taken as the experimental reference. The electrical properties of the copper oxide active layer have been measured by them as a Hall mobility and of 100 $cm^2/Vs$ and a hole concentration on the order of $10^{15}$ $cm^{-3}$. Concerning the optical properties, the wavelength dependent complex refractive index and bandgap value are extracted from ellipsometry measurements [4]. The selection of the electron affinity $\chi$ is more delicate as experimental values can take values in a wide range, from 2.9 to 4.33 eV, depending on the experimental process and the surface states of $Cu_2O$ samples [31–33]. A value of 3.2 eV is however assigned to the electron affinity in coherence with the experimental measurements and existing literature models on copper oxide [10,34,35] The densities of states $N_V$ and $N_C$ of the valence band and the conduction band respectively are calculated at room temperature $T = 300$ °C from the effective masses $m^*$ through the equation $N = 2\left(\frac{2\pi m^* k_B T}{h^2}\right)^{3/2}$, $k_B$ being the Boltzman constant and $h$ the Planck constant. The electron and hole effective masses are set to $m_e^* = 0.93 m_0$ and $m_h^* = 0.56 m_0$ respectively with $m_0$ being the electron mass [28]. The minority carrier recombination lifetimes for $Cu_2O$ have been measured to values ranging from 1 to 100 ns [30,36] and can reach up to 10 µs for high quality thermal oxide crystals with carrier concentration in the order of $5 \times 10^{14}$ $cm^{-3}$ [37]. In the model presented here, the minority and majority carrier lifetimes are set to 100 ns to match the experimental data.

### 1.2 Physical parameters of the AZO layer

The aluminum-zinc oxide layer doping concentration ($7.64 \times 10^{20} cm^{-3}$) and electron mobility ($30\,cm^2\ V^{-1}\ s^{-1}$) are set according to the measurements done on thin films

**Table 1.** Parameters of the AZO/ZnGeO/$Cu_2O$ solar cell model.

| | AZO | | $Zn_{1-x}Ge_xO$ | | $Cu_2O$ | |
|---|---|---|---|---|---|---|
| Thickness (μm) | 0.2 | [11] | 0.06 | [11] | 200 | [11] |
| $\varepsilon_r$ | 8.91 | [22] | 6.18[1] | | 7.6 | [23] |
| $E_g$ (eV) | 3.37 | [24] | 4.97[1] | | 2.034 | [4] |
| $\chi$ (eV) | 4.1 | [8] | 3.11[1] | | 3.2 | |
| $\mu_e$ ($cm^2 V^{-1} s^{-1}$) | 30 | [25] | 10 | | 200 | [10] |
| $\mu_h$ ($cm^2 V^{-1} s^{-1}$) | 3 | [26] | 5 | | 100 | [11] |
| $N_V$ ($cm^{-3}$) | $9.42 \times 10^{19}$ | [27] | $1.137 \times 10^{19}$ | | $1.05 \times 10^{19}$ | [28] |
| $N_C$ ($cm^{-3}$) | $8.09 \times 10^{18}$ | [27] | $3.718 \times 10^{18}$ | | $2.25 \times 10^{19}$ | [28] |
| Doping ($cm^{-3}$) | $7.64 \times 10^{20}$ | [25] | $10^{20}$ | | $2 \times 10^{14}$ | [11] |
| Defects Type | | | Gaussian | | | |
| $N_{DG}$ ($cm^{-3}$) | $10^{18}$ | | $10^{18}$ | | $10^{13}$ | [10] |
| Recombinations | | | | | | |
| $\beta$ ($cm^{-3}$) | $1.6 \times 10^{-10}$ | [29] | $10^{-10}$ | | $10^{-11}$ | [30] |
| $\tau_n$ (s) | $10^{-9}$ | | $10^{-9}$ | | $10^{-7}$ | |
| $\tau_p$ (s) | $10^{-9}$ | | $10^{-9}$ | | $10^{-7}$ | |

[1] Values are dependant from the germanium composition $x$ and given in this Table for $x = 0.62$ (see Sect. 1.3).

deposited by the same PLD process used for the reference solar cell [11,25]. The wavelength dependent complex refractive index of the AZO layer is deduced from ellipsometry measurements for wavelengths ranging from 200 nm up to 700 nm [38,39]. Finally, to fit the simulation results with the experimental data, the carrier lifetimes are chosen in the order of the nanosecond which is a typical value for zinc oxides [29,40] while the defect concentration $N_{DG}$ is set to $10^{18}$ $cm^{-3}$. The other physical parameters are listed in Table 1 with corresponding references.

### 1.3 Physical parameters of the buffer layer

The selection of the physical parameters of the $Zn_{1-x}Ge_xO$ (ZGO) buffer layer represents the most critical aspect of our model. Indeed, experimental data is only available for the ternary compound $Zn_2GeO_4$ and very few papers focus on other Zn/Ge ratios [41–44]. In order to simulate the solar cell structure, an estimation of the bandgap energy $E_g$, of the electron affinity $\chi$ and of the permittivity $\varepsilon_r$ are done through a linear interpolation over the whole composition range between the physical parameters of zinc oxide and germanium oxide using the following equations:

$$\begin{aligned} E_g^{ZGO} &= xE_g^{GeO} + (1-x)E_g^{ZnO} \\ \chi^{ZGO} &= x\chi^{GeO} + (1-x)\chi^{ZnO} \\ \varepsilon_r^{ZGO} &= x\varepsilon_r^{GeO} + (1-x)\varepsilon_r^{ZnO}. \end{aligned} \quad (1)$$

From the linear interpolation, the bandgap energy is estimated to be 4.97 eV for the $Zn_{0.38}Ge_{0.62}O$ compound by taking into account a 5.95 eV bandgap energy for germanium oxide [45] and a 3.37 eV bandgap energy for zinc oxide [24]. In a similar way, the interpolated electron affinity is $\chi^{ZGO} = 3.11$ eV using an electron affinity of 2.5 eV for germanium oxide [46] and 4.1 eV for zinc oxide [8]. Finally, the permittivity is calculated to a value of 6.18 from the permittivity of 4.5 of germanium oxide [47] and 8.91 of the zinc oxide [22]. It is well known that the bandgap and electron affinity dependence for ternary compounds follow a second order polynomial equation with a bowing parameter, as for instance for the ZnO/ZnS or ZnO/ZnSe systems [48]. However, without any study of the dependence of the physical parameters for the ternary compound ZGO found in the literature, the bowing parameter is unknown at the moment. Nevertheless a comparison with the $Zn_2GeO_4$ compound, the parameters of which have been previously experimentally measured to $E_g$: 4.5 eV [49,50], $\chi$: 3.80 eV [49] and $\varepsilon_r = 6.87$ [51], show that the linear interpolation used to estimate the $Zn_{0.38}Ge_{0.62}O$ parameters seems to be acceptable, even though the crystal structure of the new $Zn_{1-x}Ge_xO$ compound can differ from the binary alloys throughout the composition range.

The remaining $Zn_{0.38}Ge_{0.62}O$ parameters, namely the density of states, recombination rates, defect concentrations and doping have been selected to be similar to that of zinc oxide and adjusted to match the experimental data. They are shown in Table 1.

### 1.4 Model results and introduction of defective layers at the heterojunction

In order to validate the parameters of the model introduced in the previous section, the performances of the solar cell are evaluated for different germanium composition of the buffer layer and compared to the photovoltaic characteristics of the reference device from [11], as shown on Figure 1.

The first simulations are done without taking into account the two interface and defect layers at the junction mentioned previously and results in a maximum efficiency of 11.99% for a germanium composition of $x = 0.4$ (red curve on Fig. 1). However, the experimental optimum (black dots on Fig. 1) is achieved for a composition $x = 0.62$ with an efficiency of 6.68%.

In order to reproduce the experimental results, a 10 nm thick defective layer and 1 nm thick interface layer are included in the simulation model to account for the $Cu_2O$ defects at the junction. Both layers are defined using the same parameters as the absorber layer, except for the defect concentration of $4 \times 10^{19}$ cm$^{-3}$ for the defect layer and $1.27 \times 10^{20}$ cm$^{-3}$ for the trap levels of the interface layer. Besides the defect concentrations, the band structure of the interface layer is adjusted depending on the conduction band offset between the buffer layer and the absorber layer [52] using equations (2). The electron affinity of the interface layer $\chi^{IL}$ is set to be equal to the electron affinity of the buffer layer $\chi^{ZGO}$ while the valence band maximum of the interface layer $VBM^{IL}$ is fixed to match the valence band maximum of the absorber layer $VBM^{Cu_2O}$ (2). To prevent a negative conduction band offset between the interface layer and the absorber layer, the interface layer electron affinity is limited to a minimum value equal to the absorber electron affinity $\chi^{Cu_2O}$.

$$\chi^{IL} = \begin{cases} \chi^{Cu_2O} & \text{if} \quad \chi^{ZGO} < \chi^{Cu_2O} \\ \chi^{ZGO} & \text{if} \quad \chi^{ZGO} > \chi^{Cu_2O} \end{cases}$$
$$VBM^{IL} = VBM^{Cu_2O}. \tag{2}$$

The introduction of the interface and defect layers in the model results in a better reproduction of the experimental evolution of the solar cell performances with respect to the germanium composition, as can be seen in Figure 1. The discrepancies between the simulation results and the experimental solar cell characteristics can be explained by the approximations done to estimate the unknown physical parameters of the model and by possible differences with the experimental device, such as interfacial defect variations at the junction.

The simulated optimum efficiency of the solar cell reaches the experimental value of 6% for compositions between $x = 0.50$ and $x = 0.65$, which corresponds to a conduction band offset range of $-0.14 < \chi_{ZnGeO} - \chi_{Cu_2O} < 0.10$ eV. The open circuit voltage and short circuit current both exhibit behaviors which are coherent with the experimental data for compositions between $x = 0.50$ and $x = 0.65$. The simulation model starts to diverge from the experimental results for high germanium content ($x = 0.77$) where the solar cell performances decrease rapidly. This deviation might be due to the decrease of the electrical properties of the ZGO buffer which are not taken into account in the simulation model. Indeed, the drop of the experimental short circuit current from 9.58 mA to near 0 mA between the compositions of $x = 0.66$ and $x = 0.77$ is a strong evidence of the loss of conductivity of the buffer

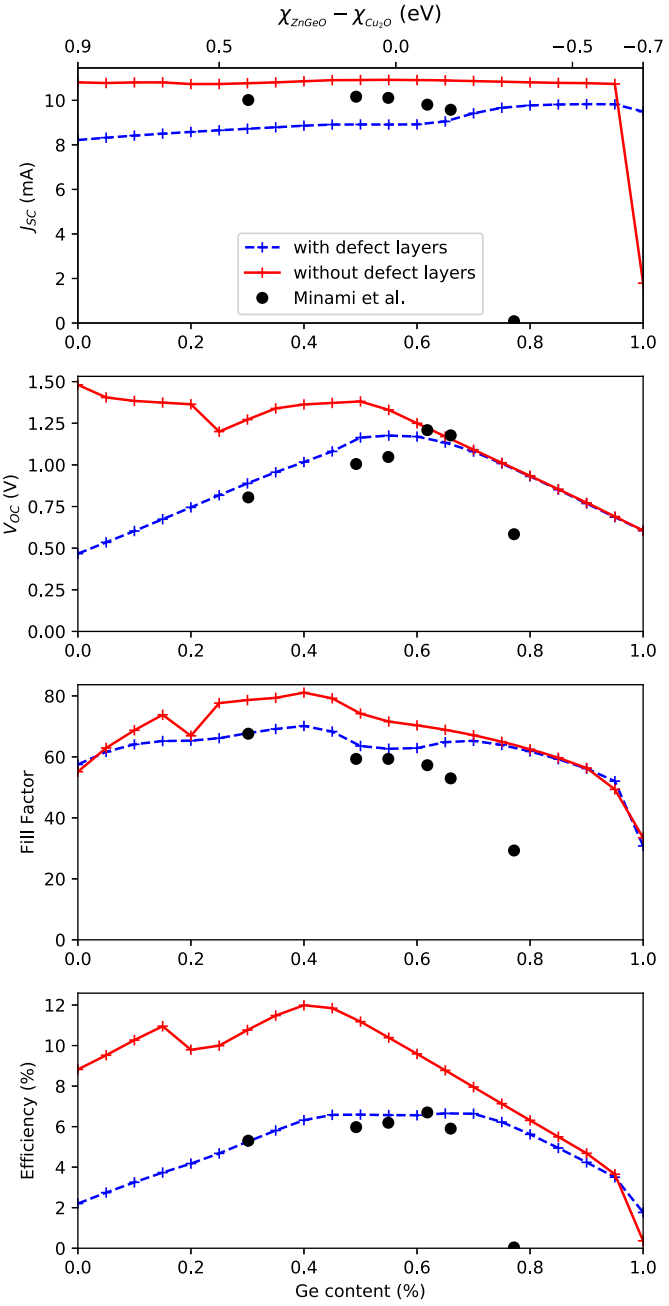


**Fig. 1.** Simulated photovoltaic characteristics of the AZO/$Zn_{1-x}Ge_xO$/$Cu_2O$ solar cell for different germanium composition $x$ or conduction band offset $\chi_{ZnGeO} - \chi_{Cu_2O}$. Simulations with (dashed blue) and without (solid red) using interfacial defect layer at the junction are compared with experimental measurements (black dots) from [11].

**Table 2.** Comparison between experimental data and simulation of the AZO/$Zn_{1-x}Ge_xO$/$Cu_2O$ solar cell with the experimental optimum germanium composition of $x = 0.62$.

| | $J_{sc}$ (mA) | $V_{oc}$ (V) | $FF$ (%) | $\eta$ (%) |
|---|---|---|---|---|
| Experimental [11] | 9.78 | 1.21 | 57 | 6.68 |
| This work (Tab. 1) | 8.94 | 1.14 | 65 | 6.61 |

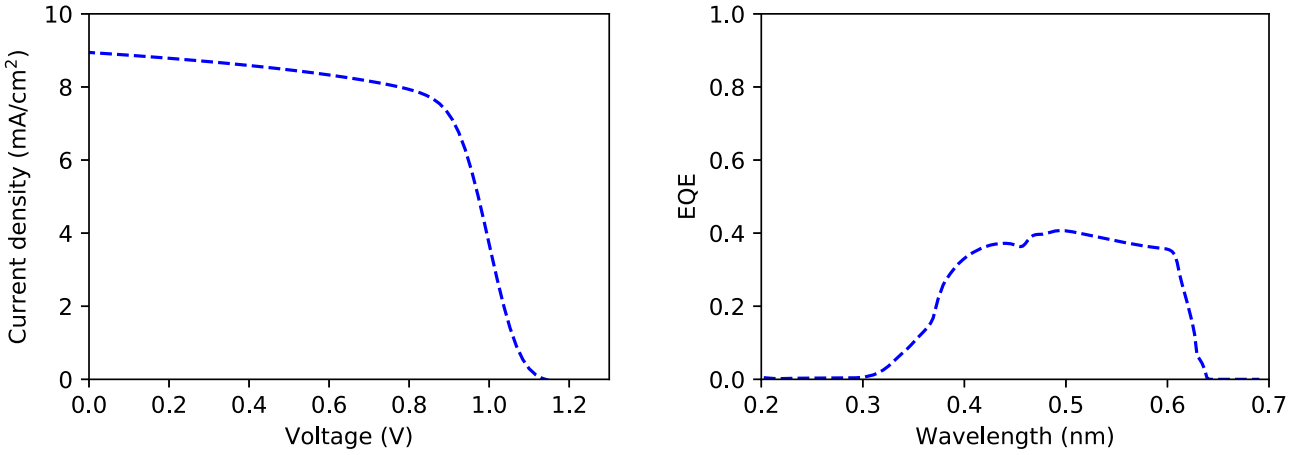


(a) (b)

**Fig. 2.** Characteristics of the AZO/$Zn_{1-x}Ge_xO$/$Cu_2O$ solar cell with a germanium composition $x = 0.62$. (a) Current-Voltage characteristics. (b) External quantum efficiency.

layer for high germanium compositions and might originate from the insulating nature of the germanium oxide.

To better compare the performances of the solar cell model with the experimental data at the optimum composition of $x = 0.62$, some numerical values are summarized in Table 2 while the simulated current-voltage and EQE characteristics are presented in Figure 2.

The ZGO/$Cu_2O$ solar cell model developed in this work allows to closely reproduce the experimental evolution of the device performances [11] as a function of the buffer layer germanium composition, confirming the importance of the conduction band alignment optimization in these new structures, in order to improve the solar cell efficiency. The device structure of the model is based on the current record $Cu_2O$ solar cell, the absorber layer of which was obtained thanks to a well controlled thermal oxidation process optimized during several decades [3].

Despite the exceptional results achieved by this elaboration process, the transposition of the technology toward the photovoltaic industry might be very challenging because of the high energy consumption of the high temperatures steps, which need to reach over 1000 °C during several hours. In order to allow large scale production with low cost and low environmental impact, research on the development of thin film metal oxides solar cells based on elaboration process compatible with the industrial standards is still required.

## 2 Absorber key parameters for the production of photovoltaic devices by spray pyrolysis

Among the undergoing investigations for the development of metal oxide solar cells, the spray pyrolysis method combines the advantages of being a low cost and large scale capable process. However, the photovoltaic devices it allows to grow still suffer from low performances with efficiencies below 1% [18,53]. In this section, the reasons for this loss of efficiency are investigated by setting the absorber physical and electrical parameters to the values they reach when the material is grown by spray pyrolysis.

### 2.1 Evolution of the solar cell performances with the absorber thickness

The main difference between the spray pyrolysis and the thermal oxidation processes concerns the absorber layer thickness. Indeed, the spray pyrolysis process being a thin film elaboration method, the $Cu_2O$ absorber layer typical thickness shrinks from 200 µm to less than 1 µm. The effect of such a reduction are investigated in this work by computing the solar cell performances for an absorber thickness varying from 200 µm to 0.5 µm, while keeping all the other parameters constants at the values that are summarized in Table 1. The results are reported in Figure 3.

A constant efficiency decrease with decreasing thickness is observed from 6.6% to 3.65%, owing to the decrease of the short circuit current. The current loss that is due to the absorber thickness reduction is linked to the decline of the light absorption in the $Cu_2O$ layer. Indeed, the maximum penetration depth $\delta = \lambda/(4\pi k)$ is larger than 10 µm for all wavelengths (200 nm $< \lambda <$ 700nm), and is thus subsequently hindered by the absorber thickness reduction below $\delta$, as confirmed in Figure 3.

However, the simulations that are summarized in Figure 3 show that despite the losses induced by the lack of light absorption in the thin film, a $Cu_2O$ solar cell made of a 1 µm thick absorber layer should exhibit a 4.20% efficiency. This is still considerably higher than the performances of similar experimental devices obtained through a spray pyrolysis process [18,19]. Therefore, the thickness of the $Cu_2O$ films grown by spray pyrolysis does not explain by itself the experimentally observed loss in efficiency, when compared to the thermal oxidation process.

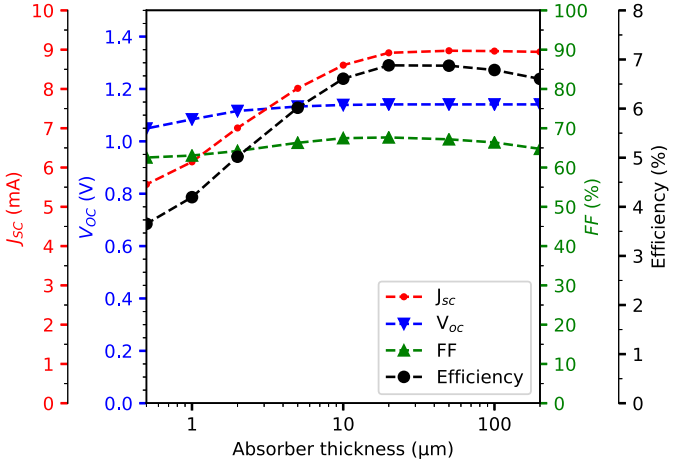


**Fig. 3.** Evolution of the solar cell performances with the absorber thickness ranging from 0.5 µm to 200 µm. $J_{SC}$ is the short cicuit current; $V_{OC}$ is the open circuit voltage; $FF$ is the fill factor.

And indeed, the use of solution based process have shown important variations in other $Cu_2O$ properties, such as carrier mobility and doping concentration, when compared to thermally oxidized materials. The following subsection is dedicated to identifying their effect on the device performances, by setting the material parameters values to that of spray pyrolysis grown $Cu_2O$.

## 2.2 Typical parameters of $Cu_2O$ by spray pyrolysis

Thin films elaborated by spray pyrolysis have been characterized by several teams to study the impact of the process parameters on their electrical properties. While the electrical properties of AZO thin films obtained by spray pyrolysis [54] are on the order of that which are obtained through classical thin film processes such as PLD, as described in Table 1, the properties of spray pyrolysis copper oxide thin films differ a lot from that of the ones obtained by thermal oxidation. Depending on the spray system, deposition conditions and doping, $Cu_2O$ thin film have shown to exhibit Hall mobilities between 0.45 and 22 $cm^2\ V^{-1}\ s^{-1}$ with carrier concentrations ranging from $2.68 \times 10^{15}$ up to $2.1 \times 10^{17}$ $cm^{-3}$ [19,55–57].

In order to evaluate, through simulation, the impact of the lower electrical properties of $Cu_2O$ obtained by spray pyrolysis, a typical value of hole mobility is chosen as $\mu_h = 5$ $cm^2\ V^{-1}\ s^{-1}$ with a doping concentration of $10^{16}$ $cm^{-3}$. The mobility ratio $\mu_e/\mu_h$ and defect concentration over doping concentration ratio are chosen similar to that of thermal copper oxide with $\mu_e = 10$ $cm^2\ V^{-1}\ s^{-1}$ and $N_{DG} = 10^{15}$ $cm^{-3}$ as no experimental data is available for spray pyrolysis samples. Using these typical electrical parameters for copper oxide obtained by spray pyrolysis and considering a 1 µm thick absorber layer, the resulting solar cell exhibits an efficiency of 3.6% ($J_{SC} = 5.14$ mA, $V_{OC} = 1.12$ V, $FF = 62.5\%$) as shown in Figure 4. The lower electrical properties of spray pyrolysis copper oxide thus do account for a loss from the 4.20% efficiency of the same device with thermal copper oxide. However, they do not account for all the loss, down to below 1%.

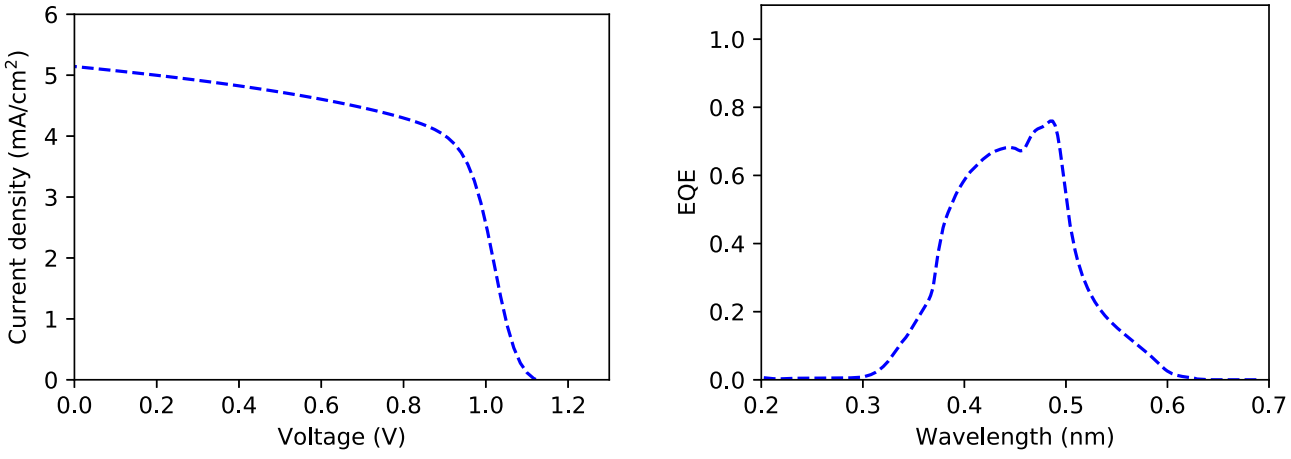


(a) (b)

**Fig. 4.** Characteristics of the AZO/$Zn_{1-x}Ge_xO$/$Cu_2O$ solar cell using typical physical parameters obtained by the spray pyrolysis process for the $Cu_2O$ absorber layer. (a) Current-Voltage characteristics. (b) External quantum efficiency.

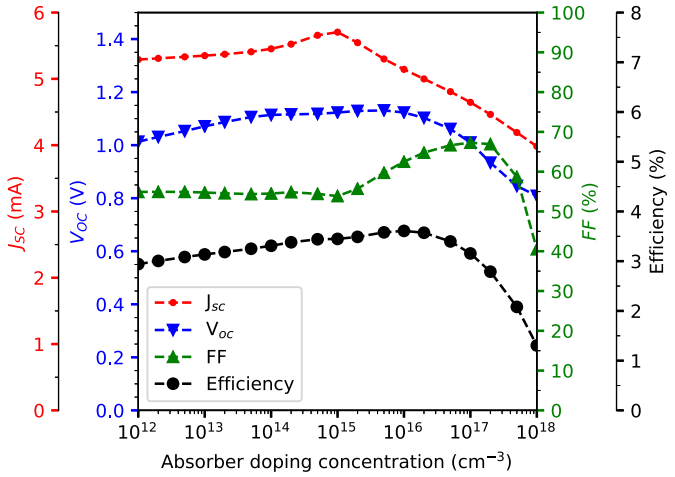


**Fig. 5.** Evolution of the solar cell performances with the doping concentration using typical physical parameters obtained by the spray pyrolysis process.

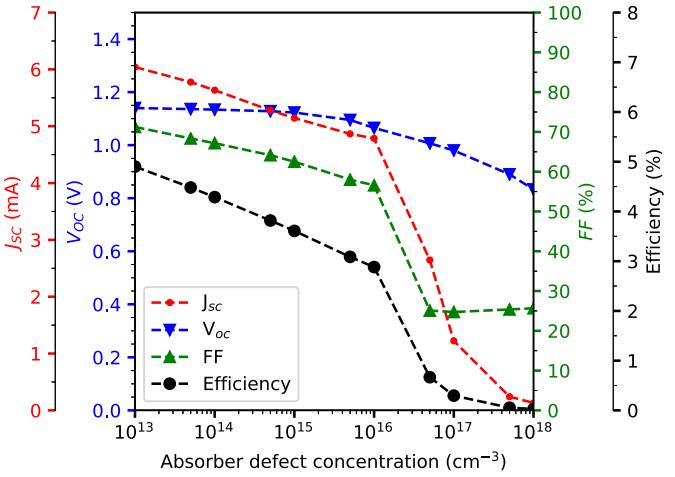


**Fig. 6.** Evolution of the solar cell performances with the defect concentration using typical physical parameters obtained by the spray pyrolysis process.

Further investigation is therefore needed. The next subsection proposes to focus on the individual impact on the solar cell performances of the mobility, the doping and defect concentrations of the $Cu_2O$ absorber layer as grown by spray pyrolysis.

### 2.3 Impact of absorber doping, carrier mobility and defect concentration on solar cell performances

The first parameter studied is the absorber doping concentration which is taken in the range from $10^{18}$ cm$^{-3}$ down to to the minimum achievable concentration of $10^{12}$ cm$^{-3}$, which can be obtained thanks to the thermal oxidation process [37]. All the other parameters are kept as defined in Section 2.2. The impact of the absorber doping on the solar cell performances is shown in Figure 5.

The simulation results show that an increase of the doping concentration beyond $10^{16}$ cm$^{-3}$ decreases both $V_{OC}$ and $J_{SC}$ and thus the efficiency, whereas, for lower values, the decrease of the doping has a limited impact. The drop in the performances for high doping concentration can be explained by the evolution of the space charge region in the absorber. At the threshold doping concentration of $10^{15}$ cm$^{-3}$, the width $w_p$ of the space charge region in the absorber reaches the maximum limit imposed by the 1 µm thickness with a value of $w_p = 0.974$ µm. Thus, for higher values of doping concentration, the decrease of the space charge region decreases the collection efficiency, while for lower doping concentration, the width of the space charge region is limited by the thickness of the layer and thus results in an optimum doping concentration on the order of $10^{16}$ cm$^{-3}$.

The results of the simulation study of the impact of the defects in the absorber layer are shown in Figure 6. The solar cell short circuit current is shown to decrease with the increase of the defect concentration. When the defect concentration exceeds the doping concentration of $10^{16}$ cm$^{-3}$, the short circuit current, and thus the efficiency of the solar cell, decrease rapidly below 1%. The defect concentration of the copper oxide layer is thus a critical parameter that must be taken care of during the elaboration by spray pyrolysis. Even though the defect concentration in the experimental devices was not estimated, the measurement of the short circuit current $J_{SC}$ was below 0.4 mA cm$^{-2}$ for the $TiO_2/Cu_2O$ heterojunction. This low value thus might originate from a high defect density and support the authors hypothesis of enhanced recombinations [18].

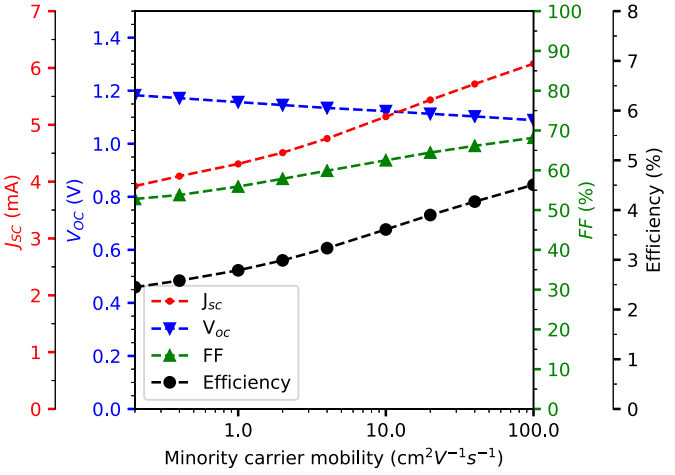


**Fig. 7.** Evolution of the solar cell performances with the carrier mobility using typical physical parameters obtained by the spray pyrolysis process.

The last parameter studied in this work is the carrier mobility. A major decrease of more than two orders of magnitude has been measured experimentally: from 200 cm$^2$ V$^{-1}$ s$^{-1}$ for $Cu_2O$ layers obtained by thermal oxidation down to less than 1 cm$^2$ V$^{-1}$ s$^{-1}$ for thin films produced by spray pyrolysis. To study the influence of the drop in the carrier mobility on the solar cell performances, simulations are performed by taking the hole mobility between 0.1 and 200 cm$^2$ V$^{-1}$ s$^{-1}$ while keeping the electron to hole mobility ratio equal to $\mu_e/\mu_h = 2$. Despite such a dramatic loss in the mobility, the numerical simulations show a limited impact on the solar cell performances, as summarized in Figure 7. Indeed, contrary to the doping or

defect concentrations, the introduction of extreme mobilities as low as $\mu_h$=1 cm$^2$ V$^{-1}$ s$^{-1}$ does not completely damage the device as the efficiency of the solar cell is still above 2.4%.

From the analysis done on the absorber layer thickness, carrier mobility, doping and defect concentrations, the path to improve the performances of $Cu_2O$ photovoltaic devices can be identified. Besides the well known limitations induced by the interfacial defects at the junction and the loss of conversion efficiency inherent to low absorber thickness of $Cu_2O$ thin film photovoltaics, a strong control of the defect distribution in the absorber layer is a key parameter to improve $Cu_2O$ photovoltaic performances obtained by spray pyrolysis. For instance, one source of defects induced by the spray pysolysis process was very recently suggested by Plankensteiner et al. [20] as impurities in the absorber layer resulting from the incomplete pyrolysis reaction of the glucose oxidizer used in the precursor solution.

Beyond the reduction of the defect density impact on the absorber layer, the present study provides useful information to define a set of parameters for the production of an efficient AZO/ZnGeO/$Cu_2O$ photovoltaic device by spray pyrolysis. This is the purpose of the next subsection.

### 2.4 Guidelines for the fabrication of high efficiency AZO/ZnGeO/$Cu_2O$ solar cell

The analysis of the $Cu_2O$ absorber parameters done in the previous subsection allows to set the requirements for optimizing a solar cell that uses it as the absorber: its carrier mobilities and layer thickness must be maximized while its defect concentration remains below the doping concentration. In this section, the absorber parameters are thus chosen to match these conditions. The absorber defect concentration is set to be ten times lower than the absorber doping concentration.

The best carrier mobility of $Cu_2O$ produced by spray pyrolysis was obtained by Ca doping with a value of 22 cm$^2$ V$^{-1}$ s$^{-1}$ [55]. Higher values such as 25 cm$^2$ V$^{-1}$ s$^{-1}$ for a 2 µm thick layer can be obtained through different elaboration processes such as sputtering [58]. Even though such performances are beyond the state of the art for $Cu_2O$ grown spray pyrolysis, other solution based processes, using other materials, have been shown to produce layer qualities that are comparable to that of sputtered thin films. This is for instance the case for aluminum zinc oxide [54,59]. Hope is thus allowed for spray pyrolysis $Cu_2O$.

In order to define some guidelines to improve the performances of future $Cu_2O$ thin film photovoltaic devices, the hole mobility are estimated to be able to reach 25 cm$^2$ V$^{-1}$ s$^{-1}$ for 2 µm thick layers when produced by spray pyrolysis. The electron mobility is set at 50 cm$^2$ V$^{-1}$ s$^{-1}$ to keep the usual hole to electron mobility ratio at 2 while the defect concentration is set at a value ten times lower than the doping concentration. Increasing the thickness beyond 2 µm might be possible and would further enhance the solar cell performances. It would however be out of the scope of thin film photovoltaics. Similarly, carrier mobilities larger than 25 cm$^2$ V$^{-1}$ s$^{-1}$ would also benefit the conversion efficiency, but reaching these values might be too challenging, owing to the polycristalline nature of the thin films that are obtained by spray pyrolysis.

Concerning the $Cu_2O$ doping concentration and germanium composition of the $Zn_{1-x}Ge_xO$ buffer layer, the optimum value to maximize the conversion efficiency might depend on the absorber layer parameters. By varying the absorber doping and germanium composition, while keeping the other model parameters at their values of Table 1, their optimum values can be identified through a numerical evaluation of the solar cell performances. These simulation results are shown by the dashed lines in Figure 8.

The simulation done using the new absorber parameters shows that the $10^{16}$ cm$^{-3}$ optimum doping defined previously in Section 2.3 is now shifted to a lower value of $10^{15}$ cm$^{-3}$. This decrease of the optimum doping can easily be explained by the possibility for the space charge region to extend beyond 1 µm with the increase of the absorber layer thickness to 2 µm. The optimum germanium composition remains centered around $x = 0.5$, in the range $0.45 < x < 0.6$. This confirms the results obtained in Section 1.4 concerning the band alignment obtained using the parameters of thermal oxidation $Cu_2O$. A new maximum of efficiency can be seen for doping concentrations below $10^{15}$ cm$^{-3}$ for a germanium composition larger than $x > 0.7$. However it is important to note that the electrical properties of the $Zn_{1-x}Ge_xO$ buffer layer defined in the model are fixed and no conductivity decrease is taken into account at high germanium content, though it might be expected because of the insulating nature of the germanium oxide.

Finally, by adjusting the absorber concentration to $10^{15}$ cm$^{-3}$ and the germanium composition to $x = 0.50$, the optimum AZO/ZnGeO/$Cu_2O$ solar cell structure is expected to reach an efficiency of 4.98% closed to the current record of 6.68% obtained by the thermal oxidation process [11].

As stated in Section 1.4, the main limitation of $Cu_2O$ solar cells originates from the defects at the heterojunction, which we modeled by the introduction of an interfacial defect layers. In order to estimate the efficiency of an ideal heterojunction, simulations are performed by removing the interfacial defects while keeping the other parameters to the expected values achievable from spray pyrolysis: an absorber layer thickness of 2 µm, hole and electron mobilities of 25 cm$^2$ V$^{-1}$ s$^{-1}$ and 50 cm$^2$ V$^{-1}$ s$^{-1}$ respectively. The impact of the buffer layer germanium composition on this ideal solar cell performances is shown by the plain lines in Figure 8 for three absorber doping concentrations, in order to identify the optimum range of composition and dopings.

In a similar way, from the devices modeled using parameters corresponding to thermal oxidation $Cu_2O$ shown on Figure 1, an increase of efficiency for the $Zn_{1-x}Ge_xO$ germanium composition below $x = 0.7$ is observed with an optimum composition of $x = 0.45$. From the study of the impact of the absorber doping concentration, the optimum value is shifted to lower doping concentration of $10^{14}$ cm$^{-3}$. Finally, in the case of an heterojunction without defective layers, an optimum efficiency of 9.57% is expected to be achievable using

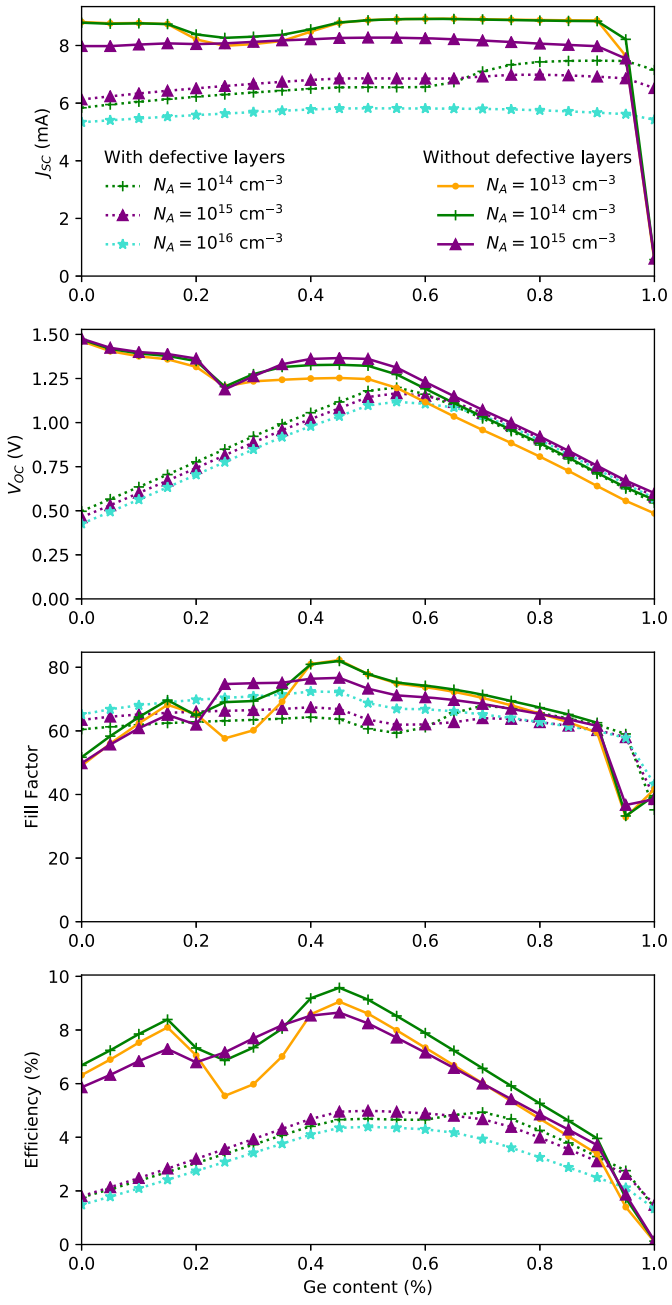


**Fig. 8.** Evolution of the solar cell performances with the germanium composition $x$ of the ZnGeO buffer layer for different absorber doping concentration $N_A$ using an absorber layer thickness of 2 µm and hole and electron mobilities of 25 cm$^2$V$^{-1}$s$^{-1}$ and 50 cm$^2$V$^{-1}$s$^{-1}$ respectively. Simulation are done using interface and defective layers at the heterojunction (dashed lines) as described in Section 1 and with an ideal heterojunction without such interface and defect layers (plain lines).

spray pyrolysis. In order to further enhance the conversion efficiency, beyond 9.57%, the solar cell structure might be improved once the all oxide technology becomes mature with, for instance, the introduction of anti-reflection coatings in order to improve light collection or back-surface field layer to decreases recombinations [34].

## 3 Conclusion

A numerical model of an AZO/$Zn_{1-x}Ge_xO$ /$Cu_2O$ photovoltaic device was developed to study the effect of the germanium composition of the buffer layer on the solar cell performances. The physical parameters of the model were chosen carefully from experimental measurements from the literature when available or through estimations from similar material when necessary. In particular, concerning the new $Zn_{1-x}Ge_xO$ compound, an interpolation of the energy levels of the band structure from the binary compounds ZnO and $GeO_2$ was calculated to allow the study the the solar cell performances over the whole germanium composition. From the solar cell model simulations, the optimum germanium composition range was identified between $x = 0.45$ and $x = 0.70$ with efficiencies higher than 6.5% thanks to the optimization of the conduction band offset in the structure. The correct match between the evolution of the simulated solar cell performances with the germanium composition and the measurements done on experimental devices confirms the high potential of the ZnGeO material to optimize the band alignment of the heterojunction and develop high performances $Cu_2O$ heterojunctions.

After this experimental validation of the solar cell simulation model, the AZO/ZnGeO/$Cu_2O$ photovoltaic device was further analysed by taking into account the constraints from thin film elaboration processes in order to benefits from the advantages of low cost, environmental friendly and industry compatible spray pyrolysis technique. Owing to the polycristalline nature of the thin films, the physical properties of $Cu_2O$ thin films are lowered if compared to the material that can be obtained by the conventional thermal oxidation process. The analysis of the solar cell performances performed using spray grown $Cu_2O$ parameters allow the definition of guidelines to improve the conversion efficiency of photovoltaic devices grown through solution based processes. Their main conclusion is that besides the well known importance of limiting the defect concentration at the junction interface originating from unwanted copper phase, the impurity levels and defect concentration of the absorber layer has to be carefully taken into account and measured to be kept at least ten times lower than the doping concentration. In order to optimize the collection efficiency of the heterojunction, the $Cu_2O$ doping should be on the order of $10^{15}$ to $10^{16}$ cm$^{-3}$ for micrometer thick absorber layers while carrier mobilities have to be at least equal to 25 cm$^2$ V$^{-1}$ s$^{-1}$.

Following the present guidelines, a simulated AZO/$Zn_{1-x}Ge_xO$ /$Cu_2O$ photovoltaic device using $Cu_2O$ parameters achievable by the spray pyrolysis process, considering the present state-of-the-art, is expected to reach efficiencies of around 5%, which is comparable to the current solar cell record based on thermal oxidation $Cu_2O$. Despite the optimized band alignement of the ZnGeO/$Cu_2O$ heterojunction and absorber layer parameters, the 5% efficiency remains low compared to the theoretical 20% Shockley-Queisser limit of $Cu_2O$ solar cells. For the development of future $Cu_2O$ based photovoltaic by spray pyrolysis, the main source of improvement relies in the

reduction of interfacial defects at the heterojunction. Indeed, the suppression of interfacial defects at the simulated ZnGeO/$Cu_2O$ heterojunction has shown devices with efficiency up to 9.57%. Besides improvements of the hetero-interface quality and in order to reach for industrial applications, the performances of spray pyrolysis $Cu_2O$ based photovoltaics will benefit from enhancements of the device structure such as introduction of anti-reflection coating [11] or back-surface field CuO layer [34] which can be developed using ultrasonic spray pyrolysis.

## Data access statement

All data created during this research is openly available from the Zenodo data archive at DOI: 10.5281/zenodo.4421835 [60].

## Conflict of interest

The authors declare no conflicts of interest.

This research was supported by "Partenariats Hubert Curien (PHC) Hibiscus" and "Lorraine Université d'Excellence (LUE)" in the framework of the "HECTOR (High EfficienCy Thin Film sOlaR cells)" research project.

## Author contribution statement

Christyves Chevallier and Sidi Ould Saad Hamady designed the simulations; Christyves Chevallier wrote the Python-related programs, Sidi Ould Saad Hamady wrote Silvaco code that was adapted by Christyves Chevallier; The experimental parameters for the Silvaco were reviewed and selected by Sourav Bose; Christyves Chevallier conducted the simulations; Sidi Ould Saad Hamady, Nicolas Fressengeas and Christyves Chevallier analyzed the simulation results; Christyves Chevallier wrote the manuscript with the input from all the authors; Nicolas Fressengeas and Sidi Ould Saad Hamady secured the financial support for the project leading to this publication; All the authors discussed the results and contributed to the final manuscript.

## References

1. A. Pérez-Tomás, A. Mingorance, D. Tanenbaum, M. Lira-Cantú, Metal oxides in photovoltaics: all-oxide, ferroic, and perovskite solar cells, in *The Future of Semiconductor Oxides in Next-Generation Solar Cells* (Elsevier, 2018)
2. S. Rühle, A.Y. Anderson, H.N. Barad, B. Kupfer, Y. Bouhadana, E. Rosh-Hodesh, A. Zaban, All-Oxide Photovoltaics, J. Phys. Chem. Lett. **3**, 3755 (2012)
3. T. Dimopoulos, All-oxide solar cells, in *The Future of Semiconductor Oxides in Next-Generation Solar Cells* (Elsevier, 2018)
4. C. Malerba, F. Biccari, C. Leonor Azanza Ricardo, M. D'Incau, P. Scardi, A. Mittiga, Absorption coecient of bulk and thin lm $Cu_2O$, Solar Energy Mater. Solar Cells **95**, 2848 (2011)
5. T. Minami, Y. Nishi, T. Miyata, Impact of incorporating sodium into polycrystalline p-type $Cu_2O$ for heterojunction solar cell applications, Appl. Phys. Lett. **105**, 212104 (2014)
6. S. Rühle, Tabulated values of the Shockley Queisser limit for single junction solar cells, Solar Energy **130**, 139 (2016)
7. C. Wadia, A.P. Alivisatos, D.M. Kammen, Materials Availability Expands the Opportunity for Large-Scale Photovoltaics Deployment, Environ. Sci. Technol. **43**, 2072 (2009)
8. C.F. Klingshirn, Zinc Oxide: from fundamental properties towards novel applications. Number 120 in Springer series in materials science, edited by C.F. Klingshirn (Springer, Heidelberg; London, 2010)
9. P. Sawicka-Chudy, M. Sibinski, E. Rybak-Wilusz, M. Cholewa, G. Wisz, R. Yavorskyi, Review of the development of copper oxides with titanium dioxide thin-film solar cells, AIP Adv. **10**, 010701 (2020)
10. Y. Takiguchi, S. Miyajima, Device simulation of cuprous oxide heterojunction solar cells, Jpn. J. Appl. Phys. **54**, 112303 (2015)
11. T. Minami, Y. Nishi, T. Miyata, Eciency enhancement using a $Zn_{1-x}Ge_xO$ thin lm as an n-type window layer in $Cu_2O$-based heterojunction solar cells, Appl. Phys. Express **9**, 052301 (2016)
12. N.H. Ke, P.T.K. Loan, D.A. Tuan, H.T. Dat, C.V. Tran, L.V. T. Hung, The characteristics of IGZO/ZnO/$Cu_2O$:Na thin film solar cells fabricated by DC magnetron sputtering method, J. Photochem. Photobiol. A: Chem. **349**, 100 (2017)
13. D. Kudryashov, A. Gudovskikh, A. Monastyrenko, All-oxide heterojunction solar cells formed by magnetron sputtering, J. Phys.: Conf. Ser. **1124**, 041017 (2018)
14. C. de Melo, M. Jullien, Y. Battie, A. En Naciri, J. Ghanbaja, F. Montaigne, J.F. Pierson, F. Rigoni, N. Almqvist, A. Vomiero et al., Semi-Transparent p-$Cu_2O$/n-ZnO Nanoscale-Film Heterojunctions for Photodetection and Photovoltaic Applications, ACS Appl. Nano Mater. **2**, 4358 (2019)
15. J. Kaur, O. Bethge, R.A. Wibowo, N. Bansal, M. Bauch, R. Hamid, E. Bertagnolli, T. Dimopoulos, All-oxide solar cells based on electrodeposited $Cu_2O$ absorber and atomic layer deposited ZnMgO on precious-metal-free electrode, Solar Energy Mater. Solar Cells **161**, 449 (2017)
16. M.H. Tran, J.Y. Cho, S. Sinha, M.G. Gang, J. Heo, $Cu_2O$/ZnO heterojunction thin-film solar cells: the effect of electrodeposition condition and thickness of $Cu_2O$, Thin Solid Films **661**, 132 (2018)
17. T. Kosugi, S. Kaneko, Novel Spray-Pyrolysis Deposition of Cuprous Oxide Thin Films, J. Am. Ceram. Soc. **81**, 3117 (1998)
18. M. Pavan, S. Rühle, A. Ginsburg, D.A. Keller, H.N. Barad, P.M. Sberna, D. Nunes, R. Martins, A.Y. Anderson, A. Zaban et al., $TiO_2$/$Cu_2O$ all-oxide heterojunction solar cells produced by spray pyrolysis, Solar Energy Mater. Solar Cells **132**, 549 (2015)
19. R. David Prabu, S. Valanarasu, V. Ganesh, M. Shkir, S. AlFaify, A. Kathalingam, Investigation of molar concentration effect on structural, optical, electrical, and photovoltaic properties of spray-coated $Cu_2O$ thin lms, Surface Interface Anal. **50**, 346 (2018)
20. N. Plankensteiner, W. Kautek, T. Dimopoulos, Aqueous Spray Pyrolysis of $Cu_2O$ Films: Inuence of Reducing Agent and Acetic Acid Addition, Chem Nano Mat **6**, 663 (2020)

21. T. Minami, T. Miyata, Y. Nishi, Relationship between the electrical properties of the noxide and p-$Cu_2O$ layers and the photovoltaic properties of $Cu_2O$-based heterojunction solar cells, Solar Energy Mater. Solar Cells **147**, 85 (2016)
22. B.K. Meyer, ZnO: dielectric constants, in *New Data and Updates for IV-IV, III-V, II-VI and I-VII Compounds, their Mixed Crystals and Diluted Magnetic Semiconductors*, edited by W. Martienssen and U. Rössler (Springer, Berlin, Heidelberg, 2011), Vol. 44D, pp. 593–593. Landolt-Börnstein - Group III Condensed Matter
23. C. Noguet, Proprietes dielectriques de l'oxyde cuivreux aux audiofrequences entre 150 K et 320 K, J. Phys. **31**, 393 (1970)
24. C. Bundesmann, R. Schmidt-Grund, M. Schubert, *Optical properties of ZnO and related compound, in Transparent Conductive Zinc Oxide*, edited by R. Hull, R.M. Osgood, J. Parisi, H. Warlimont, K. Ellmer, A. Klein, B. Rech (Springer, Berlin, Heidelberg, 2008), Vol. 104, pp. 79–124
25. T. Minami, T. Miyata, J.I. Nomoto, Impurity-doped ZnO Thin Films Prepared by Physical Deposition Methods Appropriate for Transparent Electrode Applications in Thin-lm Solar Cells, IOP Conf. Ser.: Mater. Sci. Eng. **34**, 012001 (2012)
26. B. Claflin, D. Look, S. Park, G. Cantwell, Persistent n-type photoconductivity in p-type ZnO, J. Crys. Growth **287**, 16 (2006)
27. W.M. Kim, I.H. Kim, J.H. Ko, B. Cheong, T.S. Lee, K.S. Lee, D. Kim, T.Y. Seong, Density-of-state effective mass and non-parabolicity parameter of impurity doped ZnO thin films, J. Phys. D: Appl. Phys. **41**, 195409 (2008)
28. J.W. Hodby, T.E. Jenkins, C. Schwab, H. Tamura, D. Trivich, Cyclotron resonance of electrons and of holes in cuprous oxide, $Cu_2O$, J. Phys. C: Solid State Phys. **9**, 1429 (1976)
29. S. Lettieri, L. Santamaria Amato, P. Maddalena, E. Comini, C. Baratto, S. Todros, Recombination dynamics of deep defect states in zinc oxide nanowires, Nanotechnology **20**, 175706 (2009)
30. E. Fortin, P. Rochon, J. Zielinger, Photoconductivity and photovoltaic excitation spectra and their wavelength derivative in $Cu_2O$, J. Phys. Chem. Solids **36**, 1299 (1975)
31. A. Walsh, K.T. Butler, Prediction of Electron Energies in Metal Oxides, Accounts Chem. Res. **47**, 364 (2014)
32. J. Deuermeier, J. Gassmann, J. Brötz, A. Klein, Reactive magnetron sputtering of $Cu_2O$: Dependence on oxygen pressure and interface formation with indium tin oxide, J. Appl. Phys. **109**, 113704 (2011)
33. V. Stevanović, S. Lany, D.S. Ginley, W. Tumas, A. Zunger, Assessing capability of semiconductors to split water using ionization potentials and electron anities only, Phys. Chem. Chem. Phys. **16**, 3706 (2014)
34. M.T. Rizi, M.H. Shahrokh Abadi, Numerical investigation on eciency improvement of double layer antireection coating AZO/buffer/$Cu_2O$/CuO on back-surface uorine-doped tin oxide heterostructure solar cells, J. Opt. Soc. Am. B **36**, 1155 (2019)
35. L. Zhu, G. Shao, J.K. Luo, Numerical study of metal oxide heterojunction solar cells, Semiconductor Sci. Technol. **26**, 085026 (2011)
36. A. Goltzené, C. Schwab, Impurity scattering effect on the cyclotron resonance of carriers in $Cu_2O$, Phys. Stat. Solidi **92**, 483 (1979)
37. M.A. Lloyd, S. Siah, R.E. Brandt, J. Serdy, S.W. Johnston, Y.S. Lee, T. Buonassisi. Intrinsic defect engineering of cuprous oxide to enhance electrical transport properties for photovoltaic applications, in *2014 IEEE 40th Photovoltaic Specialists Conference (PVSC)*, 2014, Vol. 2, pp. 1–3
38. K. Postava, H. Sueki, M. Aoyama, T. Yamaguchi, K. Murakami, Y. Igasaki, Doping effects on optical properties of epitaxial ZnO layers determined by spectroscopic ellipsometry, Appl. Surface Sci. **175–176**, 543 (2001)
39. H. ElAnzeery, O. El Daif, M. Buffière, S. Oueslati, K. Ben Messaoud, D. Agten, G. Brammertz, R. Guindi, B. Kniknie, M. Meuris et al., Refractive index extraction and thickness optimization of $Cu_2ZnSnSe_4$ thin film solar cells: Optimization of $Cu_2ZnSnSe_4$ thin film solar cells, Phys. Stat. Solidi **212**, 1984 (2015)
40. M. Kubota, T. Onuma, A. Tsukazaki, A. Ohtomo, M. Kawasaki, T. Sota, S.F. Chichibu, Recombination dynamics of excitons in $Mg_{0.11}Zn_{0.89}O$ alloy films grown using the high-temperature-annealed self-buffer layer by laser-assisted molecular-beam epitaxy, Appl. Phys. Lett. **90**, 141903 (2007)
41. P.R. Chalker, P.A. Marshall, P.J. King, K. Dawson, S. Romani, P.A. Williams, J. Ridealgh, M.J. Rosseinsky, Atomic layer deposition of germanium-doped zinc oxide films with tuneable ultraviolet emission, J. Mater. Chem. **22**, 12824 (2012)
42. R. Mohammadigharehbagh, S. Özen, H.H. Yudar, S. Pat, Ş. Korkmaz, Investigation of the some physical properties of Ge-doped ZnO thin films deposited by thermionic vacuum arc technique, J. Mater. Sci.: Mater. Electr. **28**, 14131 (2017)
43. R. Wang, L.L.H. King, A.W. Sleight, Highly conducting transparent thin lms based on zinc oxide, J. Mater. Res. **11**, 1659 (1996)
44. W. Zhu, T. Kammuri, S. Kitamura, M. Sturaro, A. Martucci, G. Pezzotti, Structure and composition evaluation of heavily Ge-doped ZnO nanocrystal lms, J. Phys. D: Appl. Phys. **51**, 085302 (2018)
45. T.N. Nunley, N.S. Fernando, N. Samarasingha, J.M. Moya, C.M. Nelson, A.A. Medina, S. Zollner, Optical constants of germanium and thermally grown germanium dioxide from 0.5 to 6.6eV via a multisample ellipsometry investigation, J. Vacuum Sci. Technol. B **34**, 061205 (2016)
46. L.S. Wang, H. Wu, S.R. Desai, J. Fan, S.D. Colson, A Photoelectron Spectroscopic Study of Small Silicon Oxide Clusters: $SiO_2$, $Si_2O_3$, and $Si_2O_4$, J. Phys. Chem. **100**, 8697 (1996)
47. S. Murad, P. Baine, D. McNeill, S. Mitchell, B. Armstrong, M. Modreanu, G. Hughes, R. Chellappan, Optimisation and scaling of interfacial $GeO_2$ layers for high- gate stacks on germanium and extraction of dielectric constant of $GeO_2$, Solid-State Electr. **78**, 136 (2012)
48. A. Polity, B.K. Meyer, T. Krämer, C. Wang, U. Haboeck, A. Hoffmann, ZnO based ternary transparent conductors, Phys. Stat. Solidi **203**, 2867 (2006)
49. J. Wang, C. Yan, S. Magdassi, P.S. Lee, $Zn_2GeO_4$ Nanowires As Ecient Electron Injection Material for Electroluminescent Devices, ACS Appl. Mater. Interfaces **5**, 6793 (2013)
50. X. Zhou, Q. Zhang, L. Gan, X. Li, H. Li, Y. Zhang, D. Golberg, T. Zhai, High-Performance Solar-Blind Deep Ultraviolet Photodetector Based on Individual Single-Crystalline $Zn_2GeO_4$ Nanowire, Adv. Funct. Mater. **26**, 704 (2016)

51. S. Wu, Q. Ma, Synthesis, characterization and microwave dielectric properties of $Zn_2GeO_4$ ceramics, J. Alloys Comp. **567**, 40 (2013)
52. T. Minemoto, J. Julayhi, Buffer-less Cu(In,Ga)$Se_2$ solar cells by band offset control using novel transparent electrode, Curr. Appl. Phys. **13**, 103 (2013)
53. R. David Prabu, S. Valanarasu, V. Ganesh, M. Shkir, A. Kathalingam, S. AlFaify, Effect of spray pressure on optical, electrical and solar cell eciency of novel $Cu_2O$ thin lms, Surface Coat. Technol. **347**, 164 (2018)
54. K. Ravichandran, N. Jabena Begum, S. Snega, B. Sakthivel, Properties of Sprayed Aluminum-Doped Zinc Oxide Films–A Review, Mater. Manufactur. Processes **31**, 1411 (2016)
55. S. Santhosh Kumar Jacob, I. Kulandaisamy, S. Valanarasu, A.M.S. Arulanantham, M. Shkir, A. Kathalingam, N. Soundaram, Improving the conductivity of cuprous oxide thin film by doping Calcium via feasible nebulizer spray technique for solar cell (FTO/ZnO/Ca-$Cu_2O$), Mater. Res. Express **6**, 046405 (2019)
56. W. Lan, C. Tsai, S. Lee, W. Chao, M. Shih, Y. Chou, Y. Wu, Y. Hsu, Electrical properties of cuprous oxide thin films fabricated by ultrasonic spray pyrolysis, in *2012 17th Opto-Electronics and Communications Conference*, 2012, pp. 669–670
57. K. Kardarian, D. Nunes, P. Maria Sberna, A. Ginsburg, D.A. Keller, J. Vaz Pinto, J. Deuermeier, A.Y. Anderson, A. Zaban, R. Martins et al., Effect of Mg doping on $Cu_2O$ thin films and their behavior on the $TiO_2/Cu_2O$ heterojunction solar cells, Solar Energy Mater. Solar Cells **147**, 27 (2016)
58. K. Akimoto, S. Ishizuka, M. Yanagita, Y. Nawa, G.K. Paul, T. Sakurai, Thin film deposition of $Cu_2O$ and application for solar cells, Solar Energy **80**, 715 (2006)
59. B. He, J. Xu, H. Xing, C. Wang, X. Zhang, The effect of substrate temperature on high quality c-axis oriented AZO thin lms prepared by DC reactive magnetron sputtering for photoelectric device applications, Superlatt. Microstruct. **64**, 319 (2013)
60. C. Chevallier, S. Bose, S.O.S. Hamady, N. Fressengeas, Numerical simulations of AZO/ZnGeO/$Cu_2O$ solar cells: Impact of the germanium composition of the buffer layer and the use of low cost fabrication on the photovoltaic performances, January 2021

**Cite this article as**: Christyves Chevallier, Sourav Bose, Sidi Ould Saad Hamady, Nicolas Fressengeas, Numerical investigations of the impact of buffer germanium composition and low cost fabrication of $Cu_2O$ on AZO/ZnGeO/$Cu_2O$ solar cell performances, EPJ Photovoltaics **12**, 3 (2021)